

**An integrated internet-based system for analyzing the
influence of emission sources and atmospheric
transport on measured concentrations of trace gases
and aerosols**

A. Stohl¹, J. F. Burkhart¹, S. Eckhardt¹, D. Hirdman¹, and H. Sodemann¹

¹Norwegian Institute for Air Research, Kjeller, Norway

July 2007

Available from http://zardoz.nilu.no/~andreas/publications/web_based_tool.pdf

Norwegian Institute for Air Research
Instituttveien 18, 2027 Kjeller, Norway

Abstract

Analysis of the measured atmospheric concentrations of greenhouse gases, pollutants, aerosols or radioactive substances often requires information on the air mass transport and upwind emission sources. Historically, this information could only be obtained from calculated back trajectories. However, even though more advanced atmospheric transport models (backward-running Lagrangian particle dispersion models, adjoint chemistry transport models) are now available, the experimentalists still mostly use the simple but less accurate trajectory models. Tools that help the researchers with the interpretation of the rather complex output produced by the more advanced models are essential to improve this situation in the future. In this note we introduce a new internet-based system, which provides a suite of products derived from the output of a backward-running Lagrangian particle dispersion model. To enhance its value, the model output has been integrated with other information such as anthropogenic emission inventories and biomass burning fire detections. We expect that systems like this will soon replace the simple trajectory models for most applications.

1 Introduction

For decades, trajectory models such as HYSPLIT (Draxler and Rolph, 2003; Draxler, 2003), FLEXTRA (Stohl et al., 1995), LAGRANTO (Wernli and Davies, 1997), TRAJKS (Scheele et al., 1996) or the NASA/Florida State University model (Fuelberg et al., 1996) have been the main tools for analyzing the transport of radioactive constituents, air pollutants and greenhouse gases from their sources to observation sites. The HYSPLIT model, for instance, can even be run over the internet (see http://www.arl.noaa.gov/ready/hysp_info.html) and, therefore, became very popular among experimentalists. Other models such as FLEXTRA are run operationally for a large number of sites (see <http://www.nilu.no/trajectories/>). In order to discern the pollutant¹ sources, the models are typically run backward in time from a measurement site, resulting in so-called back trajectories (Stohl, 1998).

Unfortunately, trajectory models provide rather qualitative information and they ignore turbulence and convection, which are important processes especially near the Earth's surface (Stohl et al., 2002). The complexity of dispersion in the atmosphere can be better accounted for with Lagrangian particle dispersion models (LPDMs) or Eulerian chemistry transport models (CTMs). For the interpretation of in-situ point measurements, these models are most effectively run in a receptor-oriented mode (i.e., backward in time), like the simple trajectory models (Seibert and Frank, 2004). In the Eulerian framework, this requires using an adjoint model (Issartel and Baverel, 2003). LPDMs are basically self-adjoint (Flesch et al., 1995), except for the sign of the advection and some minor forward/backward asymmetries for skewed turbulence and convection (Seibert and Frank, 2004). LPDMs are particularly attractive tools for interpreting measurement data, as they can be run backward from a point measurement site. CTMs are bound to their respective grid resolution and also suffer from numerical diffusion, which may overwhelm the physical diffusion. However, in principle, both model types are capable of producing the same type of information: they can map quantitatively the sensitivity of the pollutant concentration at the receptor site to emission input as a function of space and time. This is possible for inert species and substances with first-order loss processes (e.g., radioactive decay, dry deposition, wet scavenging, or linear chemical conversion). Example applications of this type can be found, for instance, in Stohl et al. (2003, 2007a) for the LPDM FLEXPART, Lin et al. (2003) for the LPDM

¹Throughout the paper we use the term "pollutant" in a generic sense for any trace constituent of the atmosphere; it can also stand for a radionuclide or a greenhouse gas, for instance.

STILT, or Issartel and Baverel (2003) for the CTM POLAIR.

LPDMs and CTMs that are capable of running backward in time have been available for more than a decade (Flesch et al., 1995; Pudykiewicz, 1998), and computing resources are no longer an obstacle for using them. Surprisingly, however, the majority of experimentalists do not take advantage of their superior accuracy. Instead, they still use simple back trajectories for interpreting their measurement data. We believe this points towards a communication problem between the modelers and the experimentalists that is partly related to the complexity of the adjoint model output. While a trajectory can be plotted as a single line on a map, the equivalent output of an adjoint LPDM or CTM calculation is a four-dimensional field, which cannot be displayed so easily. Data sharing between modelers and experimentalists is difficult because of the relatively large data volumes. Statistical analyses of LPDM or CTM results are also more demanding than for trajectories but certainly possible as has been shown by Han et al. (2005). To facilitate the data analysis, powerful post-processing tools are required to extract and display the relevant information from such a complex model output. These post-processing tools also need to incorporate emission information in order to take full advantage of the model output.

The purpose of this note is to introduce an integrated system that we have developed for making backward transport model results attractive for experimentalists and which is already becoming increasingly popular among them. The system is an internet-based front-end for displaying the output from the LPDM FLEXPART but it is not specific to that model. In fact, FLEXPART could easily be exchanged with some other backward-running LPDM or adjoint CTM. This note does not describe the theory behind the model calculations. For that, we refer the reader to the paper by Seibert and Frank (2004), which we strictly follow. However, to facilitate communication with the experimentalists, we have simplified some of the terminology used by these authors.

The integrated system has been developed for a number of large measurement campaigns and research sites, for which it is now available. The setup of the system slightly varies between these campaigns but the overall concept and available products are as described in this note. In the following, we first briefly describe the underlying model calculations, then we illustrate the system's functionality, and finally we explain the different products accessible.

2 Model calculations

2.1 Meteorological input data

All model simulations are based on meteorological analysis or re-analysis data at six-hourly intervals (0, 6, 12, 18 UTC) and 3-hour forecasts at intermediate times (3, 9, 15, 21 UTC). For all campaigns, data from the European Centre for Medium-Range Weather Forecasts (ECMWF) (White, 2002) with $1^\circ \times 1^\circ$ resolution have been used. Their vertical resolution is between 60 and 91 levels, depending on the available ECMWF data. Nests with 0.25 to 0.36° resolution have been used in the areas of main interest for most of the measurement campaigns but not for the multi-annual calculations made for monitoring stations. For the campaigns, we have also made alternative simulations using data with $1^\circ \times 1^\circ$ resolution and 26 levels from the Global Forecast System (GFS) model of the National Center for Environmental Prediction (NCEP).

2.2 Model description and model output

All model calculations have been made with the LPDM FLEXPART. For a description of the model, see Stohl et al. (1998); Stohl and Thomson (1999); Stohl et al. (2005) and the internet webpage at <http://transport.nilu.no/>. In brief, FLEXPART calculates the trajectories of so-called tracer particles using the mean winds interpolated from the meteorological input fields plus random motions representing turbulence. For moist convective transport, FLEXPART uses the scheme of Emanuel and Živković-Rothman (1999), as described and tested by Forster et al. (2007).

The integrated system is based on backward (adjoint) calculations (Stohl et al., 2003; Seibert and Frank, 2004) from a measurement site (receptor) for the volume mixing ratio of a generic inert tracer with infinite lifetime. A generic inert tracer is considered most appropriate when experimentalists are interested in a wide range of gases and aerosols with vastly different properties, as it is typical for large campaigns. It also allows visualizing the atmospheric transport of the sampled air mass similar to a back trajectory (see below). Nevertheless, in the future we will add another generic tracer that is subject to washout and dry deposition.

For every receptor, 40000 particles are released in a small box at the measurement location and during the measurement interval (see below) and followed backward in time for 20 days. The cloud of particles forms a so-called retroplume (Issartel and Baverel, 2003),

in analogy to the plume forming downwind of a point source in a forward simulation. The model output is a three-dimensional potential emission sensitivity (PES) distribution, as described by Seibert and Frank (2004) who called this quantity source-receptor relationship. We prefer the term PES, as it indicates that an adjoint simulation is essentially a sensitivity analysis. The word "potential" shall remind the user that the sensitivity is based on transport calculations for an inert substance, ignoring removal processes that would reduce the sensitivity. The value of the PES (in units of s kg^{-1}) in a particular grid cell is proportional to the particle residence time in that cell. It is a measure for the simulated mixing ratio at the receptor that a source of unit strength (1 kg s^{-1}) in the respective grid cell would produce.

The PES output is made on a three-dimensional grid of typically 1° longitude \times 1° latitude resolution and global or hemispheric coverage. In the region of largest interest for a given campaign, we normally also use a nested output grid of 0.25° to 0.5° resolution. Only a few (3-5) vertical layers are used, with most layers below 3000 m, and the uppermost layer covering the rest of the atmosphere. Model output is produced every 24 hours, such that the PES distribution in time is also known.

In addition to the gridded model results, we also perform a cluster analysis of particle locations, and write the cluster centroid positions of five clusters to output files. Furthermore, we also report the fraction of all particles residing in the boundary layer and the fraction residing in the stratosphere. This model output is described in Stohl et al. (2002) and is used for a special type of retroplume summary plot (see below).

2.3 Selection of model calculations

All displayed products are derived from backward model calculations that have been initialized in boxes covering the volume of a measurement and during the time period of the measurement. Some of the measurements have a very high time and/or space resolution and, thus, a certain data reduction is necessary in order to keep the number of required model calculations manageable. The exact criteria applied for this have been slightly different for the various data sets and are specified on the internet pages for the individual campaigns. However, we distinguish three cases with the following typical criteria:

- Surface stations: Model calculations are initialized every 3 hours from the point located exactly at the measurement site. Particles are released at a uniform rate during a 3-hour interval, such that the model results can be compared with 3-hour mean

measurements.

- Vertical soundings: Interesting profiles are selected, and model calculations are initialized in an array of vertical layers of typically 250-500 m width each. The particles are released either instantaneously or during a certain time interval at the exact position of the sounding site.
- Mobile platforms (aircraft or ships): Every flight or ship track is split into small segments, typically a few hundred, depending on the position changes of the platform. A new segment is generated whenever the platform has moved by more than 0.15° in either longitude or latitude, or when it has changed its altitude by more than 10 hPa. Also, at least one calculation is made every hour, even when the platform does not move. The particles are released in four-dimensional boxes covering the longitude, latitude and altitude range as well as the time period of a segment.

3 The internet-based integrated backward-transport-modeling system

The integrated system is accessible via the webpage <http://transport.nilu.no/products>. FLEX-PART model output for several large campaigns and various monitoring stations has been integrated into a web portal for display of the derived products described below. By design, we have developed the software to use simple HTML (Hypertext Markup Language) for fast browsing calling upon pre-generated plots for periods of interest. As for each campaign and site there are up to several million different plots generated, browsing these results can be overwhelming. The idea behind this portal is to provide an innovative user interface allowing quick retrieval of periods of interest for analysis, and a convenient way of comparing the various available model products.

3.1 Navigation of the internet webpages

From the portal entry, the user first needs to go to the campaign or site overview page. This page lists all data sets that have been produced for that campaign or site. As an example, Fig. 1 shows the homepage that was produced for a number of concurrent campaigns conducted in spring 2006. By selecting a data set of interest (i.e., a certain flight, profile, or surface station) a list of all available model products is provided (see Fig. 2).

Selecting a model product brings up a list of available times of model output. Once a time

has been selected, the user is brought to our main browser, receiving the selected plot with a number of navigation links. Figure 3 shows an example after selecting a column-integrated PES. The various products available are described in the next section, here we provide an overview of the site navigation.

Using the navigation links, the user can go back to the campaign overview page ("HOME") shown in Fig. 1 or to the list of products available for the respective data set (flight, etc.) ("AVAILABLE PRODUCTS FOR THIS FLIGHT") as shown in Fig. 2. If model calculations have been made both with ECMWF and GFS input data, the user can toggle between the two ("PLOT USING GFS DATA"). When changing the model input data the time remains the same, facilitating an easy comparison between the two alternative simulations and, thus, allowing an identification of cases with large uncertainties.

The user can also swap between the different available model products (links shown in the line "CHANGE TYPE OF PLOT"), which are explained in the next section. Again, when changing the plot type the time remains the same, such that one can, for instance, explore how a change in the column-integrated PES affects the potential source contributions.

Another option offered is to change the plotting region. Most types of plots have been produced for three regions: a global domain, a regional zoom showing the area where a large influence from emissions is expected, and then either a polar stereographic view or a local zoom into the region where the measurements have been made. The global and polar stereographic plots are based on the global model output, whereas the regional and local zooms use the nested model output with higher resolution.

Finally, the user can also navigate in time, i.e. either go back ("PREVIOUS") or advance ("NEXT") along the data set (e.g., a flight). This is particularly useful for quickly browsing through the data set to see how the various model products change with time, for instance as an aircraft performs a vertical profile. Alternatively, the user can also go back to the list of all available times ("OVERVIEW").

3.2 Available model products

3.2.1 Column-integrated potential emission sensitivity (PES)

We generally recommend to start the browsing with the column-integrated PES (Fig. 3), i.e. the PES integrated over the entire atmospheric column. While it does not give any information on the PES altitude distribution, it reveals the major geographical pathway(s)

along which the air has traveled to the receptor. Of all our products, the column-integrated PES plot is probably most comparable to a traditional trajectory plot. The receptor point is marked by an asterisk and the numbers plotted on top of the contours are the daily retroplume centroid positions (explained in detail later), which roughly indicate the transport speed, at least for the last days before arrival at the receptor. As an example, Fig. 3 shows a regional view of the transport of air from Eastern Europe to the Zeppelin research station on Spitsbergen, a case recently discussed by Stohl et al. (2007b). The air arrived along a distinct and rather narrow path indicated by the reddish colors, which is reminiscent of a classical back trajectory. However, as the corresponding global plot reveals, the retroplume eventually splits into multiple pathways, yielding a relatively high column-integrated PES across much of the latitudes north of 50°N . This is typical for the relatively long transport times of up to 20 days accounted for in our calculations. In many other cases a single transport pathway is not evident even during the first few days.

Also shown in Fig. 3 are the locations of satellite detections of active fires (black dots). These detections are based on MODIS (Moderate Resolution Imaging Spectroradiometer) Collection 4 data and the MOD14 and MYD14 algorithms (Giglio et al., 2003) (see http://maps.geog.umd.edu/products/MODIS_Fire_Users_Guide_2.2.pdf). The fires are shown only if the daily (not total) column-integrated PES in the respective grid cell exceeds 8 ns m kg^{-1} on the day of detection. This ensures that only fires are shown which were detected on days when a significant fraction of the air mass arriving at the receptor was transported over them. A high-resolution land cover inventory (Hansen et al., 2000) is used to determine the dominant land cover type at the location of a fire detection. When the dominant land cover is some kind of forest, a small red dot is superimposed on the larger black dot, as emissions from forest fires can potentially be much larger than emissions from agricultural fires. In the example shown (Fig. 3), there are many fires (mostly on agricultural land) detected in the pathway of the air arriving at Zeppelin, which suggests a substantial contribution of biomass burning emissions to pollutant concentrations at Zeppelin (Stohl et al., 2007b).

The MODIS fire detections are not yet available to us for all campaigns/data sets shown. However, we are in the process of re-producing many of the webpages using the ATSR (Along-Track Scanning Radiometer) fire detections, which are available since the year 1995 (Arino and Melinotte, 1998).

3.2.2 Footprint potential emission sensitivity (PES)

Most of the anthropogenic emissions occur at or near the Earth's surface, which means that high PES values near the surface are generally more important than high PES values in the upper layers of the atmosphere. Therefore, we present plots of the PES in the lowest model layer, for most data sets 0-100 m above the ground, which we call the "footprint PES", in analogy to the footprint for flux measurements, which is a commonly used term in micrometeorology (see, e.g., Flesch, 1996). The results are not very sensitive to small changes in the footprint layer height, as long as this height is lower than the atmospheric boundary layer height. A greater height leads to better particle counting statistics in FLEXPART and, thus, less noisy results, whereas a lower height is somewhat more appropriate to describe the PES for surface emissions. The 0-100 m footprint layer height is a good compromise for the number of particles we currently use (40000).

In the footprint PES plots, fire detections are shown in grid cells where the daily footprint emission sensitivity on the very day of the fire detection is above 5 ps kg^{-1} . As the altitude of smoke injection into the atmosphere can vary, we recommend inspecting both the footprint and column-integrated PES over regions with active fires.

Figure 4 shows, as an example, the PES in the footprint layer for the same case as presented before. Since the measurement station is at the ground, the footprint PES stretches back right from the station. If the receptor is at higher altitude (e.g., for an aircraft measurement), the retroplume sometimes touches down into the footprint layer only thousands of kilometers away, leading to zero PES in the immediate surroundings of the receptor. In the present case, high values of the PES stretch back from the receptor to the region of biomass burning in Eastern Europe. Outside this major retroplume pathway, PES values are close to zero. This indicates that the "background" of moderately large values of the column-integrated PES north of about 50°N seen in Fig. 3 is mostly due to PES at higher altitudes.

3.2.3 Potential source contributions (PSC)

Anthropogenic PSC: To reveal the potential contribution from anthropogenic pollution sources, we fold (i.e., multiply) the PES footprint with the emission flux densities (in units of $\text{kg m}^{-2} \text{ s}^{-1}$) taken from an appropriate emission inventory (see below). The resulting potential source contribution (PSC) plot (in units of ppbv m^{-2}) shows the geographical

distribution of sources contributing to the simulated mixing ratio at the receptor. Spatial integration finally gives the simulated total mixing ratio at the receptor which is also reported on the plot. For species that are conserved on the time scales considered here (e.g., carbon monoxide), this total mixing ratio should be quantitatively comparable to the measured enhancement over an eventual background. In addition, the contributions from the different continents, obtained by regional integration, are also listed on the plot.

We calculate PSC maps for three tracers: carbon monoxide (CO), nitrogen oxides (NO_x, calculated as NO₂) and sulfur dioxide (SO₂). Note that the underlying emission sensitivities have been calculated for an inert substance and, thus, CO, NO_x and SO₂ are treated in the same way. Differences occur only as a result of their different emission distributions. We take the emission fluxes from the global EDGAR 3.2 Fast Track 2000 dataset (Olivier et al., 2001) and blend this global inventory with higher-resolution regional inventories where available: for instance, a North American inventory from Frost et al. (2006), and a European inventory from the UNECE/EMEP (United Nations Economic Commission for Europe/Co-operative Programme for Monitoring and Evaluation of Long Range Transmission of Air Pollutants in Europe) emission database (Vestreng et al., 2005).

In Fig. 5 we show the CO PSC for the same case as discussed already above. Non-zero values of the PSCs can be found mostly where the footprint PES is high (compare with Fig. 4). However, there is a strong modulation by the actual distribution of emissions and high values can only be found in a single region, namely Moscow, where both the emission fluxes and the footprint PES are relatively large. The total simulated CO mixing ratio at the receptor, 9.6 ppbv, is moderate. Observe that for regional and local plots PSCs are integrated only over the nested domain, such that reported mixing ratios on these plots do not include contributions from outside the nested domain.

Biomass burning PSC: PSCs are also calculated for CO from biomass burning. The algorithm used for estimating emission fluxes is described in Stohl et al. (2007b) and is essentially based on satellite fire detections, a statistical relationship between the area burned and the number of detected fires, a land cover inventory, and assumptions for the biomass per area, the fraction of it consumed by the fire, and CO emission factors for the different land cover types. Otherwise, PSC maps are produced in exactly the same way as for the anthropogenic emissions. Figure 6 shows the biomass burning CO PSC map for the same case as discussed previously. Large contributions can be seen from the area where many fires were detected (compare with Fig. 4), giving a total simulated biomass burning CO mixing

ratio of 71 ppb at Zeppelin.

3.2.4 Retroplume summary plots

The retroplume summary plots display the complex structure of a retroplume in a single plot, based on a technique described by Stohl et al. (2002). The retroplume's daily centroid positions are connected with a line, which gives the plot an appearance similar to a classical trajectory plot (see Fig. 7 for our example case). As the retroplume becomes complex back in time, the total centroid may not be representative anymore of the true retroplume location and shape. For instance, imagine a banana-shaped retroplume where the centroid would lie outside the entire retroplume. Nevertheless, often the centroid is quite representative for at least a few days back and, thus, daily retroplume centroid positions are plotted as numbers also in all other product plots (e.g., Fig. 3), giving at least a rough indication of the transport speed.

During the model calculation, particles are also clustered into five groups according to their position. For every daily cluster centroid, a circle is drawn on the retroplume summary plot (see Fig. 7), with the circle's radius scaled with the number of particles belonging to that cluster. A circle's color indicates the cluster mean altitude, and the number on top gives the time backward in days. Thus, this plot summarizes the retroplume's shape both in three-dimensional space and in time.

In three more panels of the retroplume summary plot (Fig. 7), certain retroplume characteristics are shown as a function of travel time. Firstly, the retroplume total centroid and cluster centroid altitudes are plotted as a line and as circles, respectively. Secondly and thirdly, the fraction of particles in the boundary layer and the fraction of particles in the stratosphere (potential vorticity (PV) greater than 2 PV units polewards from 30°, thermal tropopause in the tropics) are shown. This can be used, for instance, to estimate the impact of transport of stratospheric ozone on tropospheric ozone measurements (see, e.g., Cooper et al., 2006). Fig. 7 is not a particularly illustrative example of a retroplume summary plot, as the retroplume remained at rather constant altitude but was chosen here as an example nevertheless, for consistency with the other model products shown.

3.2.5 Time series of age spectra and continental source contributions

Spatial integration of a PSC map (see Fig. 5) yields a calculated mixing ratio at the receptor. Furthermore, as the timing of the PSCs is also known, the mixing ratio can be displayed as

a function of the time elapsed since the emission has occurred (i.e., "age"). This leads to an age spectrum, which can be shown as stacked bars, where a bar's color indicates the contribution of a certain age bin (0-1 days, 1-2 days, ..., 19-20 days). As this can be done for all times of a given data set, the age spectra can be shown as a time series of colored stacked bars.

Figure 8 shows the age spectra time series for the biomass burning CO at the Zeppelin research station for the month of May 2006. The pollution episode during the first days of May 2006 is clearly evident in Fig. 8. This also highlights another advantage of the integrated system: Since the model results can be compared with measured time series of long-lived tracers (e.g., CO), the model's skill can be checked. Cases where an observed event is not reproduced by the model can be identified and point either to a source missing in the emission inventories used, or to errors in the simulated transport. This important quality check cannot be done when using classical trajectories.

If a platform (e.g., an aircraft) changes its altitude, the altitude time series is superimposed on the time series plot as a black line, such that the age spectra can easily be related to characteristic altitude changes (e.g., vertical profiles). If the data set is a single vertical profile, the age spectra are shown as a function of altitude instead of time. The webpage also contains a link (see Fig. 8) to a plain text file containing the data underlying the age spectra plot. Experimentalists can conveniently use these data to plot the simulated mixing ratios together with their measurements, or for statistical analyses.

The age spectra plots are available not only for biomass burning CO, but also for anthropogenic emissions (CO, NO_x, SO₂). Furthermore, since PSC maps can be integrated also regionally, there are plots and data files for anthropogenic emissions from every individual continent, plus a plot showing the anthropogenic contributions color coded not as a function of age but for regional origin. These plots are similar to Fig. 8 and, thus, are not shown here.

4 Outlook

The philosophy underlying the integrated system described in this note is that of an interactive system which allows a user efficient browsing of pre-generated model output. The user can only select from the available plots. However, we store all the model output and customized high-quality plots can be produced on personal request.

In the future, the system could be developed towards a dynamic one, where the user

submits a request triggering a model simulation and returning the data, browse pages and user-defined plots. While this is technically possible, the current system has other advantages. Through active involvement of our group in measurement campaigns and by running the model and plotting routines partly manually, the products undergo a quality control before being released to the public. We certainly cannot check every single plot and, admittedly, for some data sets a few plots are missing (e.g., because of difficulties with the plotting software). However, a minimum standard is guaranteed. Whenever possible, we incorporate information specific to the campaigns, for instance local emission inventories, or high-resolution ECMWF input data for the region of interest. Our active involvement also ensures that the data entered into the system are quality controlled and of optimum quality. The same quality would be very difficult to achieve with a fully dynamic system. Furthermore, required data volumes are large and computation times are relatively long even with currently available technology. Thus, a fully automated system working without too many restrictions for the users would be operationally expensive in order to provide any kind of reasonable response time. Therefore, we foresee that the current system will be further developed and used for many years. A user-driven system may be developed in addition to it, but certainly not as a replacement.

Finally, we would like to encourage experimentalists interested in the system to contact us. Even though our resources are limited, we are willing to set up the system also for other campaigns and measurement sites.

Acknowledgements. This study was done as part of three projects: EUCAARI (European integrated project on aerosol cloud climate and air quality interactions) funded by the European Union, and POLARCAT-Norway (Polar study using aircraft, remote sensing, surface measurements and models, of climate, chemistry, aerosols, and transport) as well as SUMSVAL (A comparison of data from atmospheric research stations at Summit, Greenland, and Zeppelin, Spitsbergen), funded by the Norwegian Research Council. A. Stohl acknowledges discussions with P. Seibert on the theory of backward modeling.

References

- Arino, O. and Melinotte, J.: The 1993 Africa fire map, *Int. J. Remote Sens.*, 19, 2019–2023, 1998.
- Cooper, O. R., Stohl, A., Trainer, M., Thompson, A. M., Witte, J. C.: Large upper tropospheric ozone enhancements above midlatitude North America during summer: In situ evidence from the IONS and MOZAIC ozone monitoring network, *J. Geophys. Res.*, 111, D24S05, doi:10.1029/2006JD007306, 2006.
- Draxler, R. R., and Rolph, G. D.: HYSPLIT (HYbrid Single-Particle Lagrangian Integrated Trajectory), Model access via NOAA ARL READY Website NOAA Air Resources Laboratory, Silver Spring, MD, <http://www.arl.noaa.gov/ready/hysplit4.html>.
- Draxler, R. R.: Evaluation of an ensemble dispersion calculation, *J. Appl. Meteorol.*, 42, 308–317, 2003.
- Emanuel, K. A., and Živković-Rothman, M.: Development and evaluation of a convection scheme for use in climate models, *J. Atmos. Sci.*, 56, 1766–1782, 1999.
- Flesch, T. K., Wilson, J. D., and Lee, E.: Backward-time Lagrangian stochastic dispersion models and their application to estimate gaseous emissions, *J. Appl. Meteorol.*, 34, 1320–1333, 1995.
- Flesch, T. K.: The footprint for flux measurements, from backward Lagrangian stochastic models, *Bound.-Lay. Meteor.*, 78, 399–404, 1996.
- Forster, C., Stohl, A., and Seibert, P.: Parameterization of convective transport in a Lagrangian particle dispersion model and its evaluation, *J. Appl. Met. Clim.*, 46, 403–422, 2007.
- Frost, G. J., McKeen, S. A., Trainer, M., Ryerson, T. B., Neuman, J. A., et al.: Effects of changing power plant NO_x emissions on ozone in the eastern United States: Proof of concept, *J. Geophys. Res.*, 111, D12306, doi:10.1029/2005JD006354, 2006.
- Fuelberg, H. E., Loring Jr., R. O., Watson, M. V., Sinha, M. C., Pickering, K. E., Thompson, A. M., Sachse, G. W., Blake, D. R. and Schoeberl, M. R.: TRACE A trajectory intercomparison. 2. Isentropic and kinematic methods, *J. Geophys. Res.*, 101, 23927–23939, 1996.
- Giglio, L., Descloitres, J., Justice, C. O., and Kaufman, Y.: An enhanced contextual fire detection algorithm for MODIS, *Rem. Sens. Environ.*, 87, 273–282, 2003.
- Han, Y. J., Holsen, T. M., Hopke, P. K., Yi, S. M.: Comparison between back-trajectory based modeling and Lagrangian backward dispersion modeling for locating sources of reactive gaseous mercury, *Environ. Sci. Tech.*, 39, 1715–1723, 2005
- Hansen, M., DeFries, R., Townshend, J. R. G. and Sohlberg, R.: Global land cover classification at 1 km resolution using a decision tree classifier, *Intern. J. Rem. Sensing.*, 21, 1331–1365, 2000.
- Issartel, J.-P., and Baverel, J.: Inverse transport for the verification of the Comprehensive Nuclear Test Ban Treaty, *Atmos. Chem. Phys.*, 3, 475–486, 2003.
- Lin, J. C., Gerbig, C., Wofsy, S. C., Andrews, A. E., Daube, B. C., Davis, K. J., and Grainger, C. A.: A near-field tool for simulating the upstream influence of atmospheric observations: The

- Stochastic Time-Inverted Lagrangian Transport (STILT) model, *J. Geophys. Res.*, 108, 4493, doi:10.1029/2002JD003161, 2003.
- Olivier, J. G. J. and Berdowski, J. J. M.: *Global emissions sources and sinks*, In: Berdowski, J., Guicherit, R. and Heij, B. J. (eds.) "The Climate System", pp. 33-78. A.A. Balkema Publishers/Swets & Zeitlinger Publishers, Lisse, The Netherlands. ISBN 90 5809 255 0.
- Pudykiewicz, J.: Application of adjoint tracer transport equations for evaluating source parameters, *Atmos. Environ.*, 32, 3039–3050, 1998.
- Scheele, M. P., Siegmund, P. C., and Velthoven, P. F. J.: Sensitivity of trajectories to data resolution and its dependence on the starting point: in or outside a tropopause fold, *Meteorol. Appl.*, 3, 267–273, 1996.
- Seibert, P. and Frank, A.: Source-receptor matrix calculation with a Lagrangian particle dispersion model in backward mode, *Atmos. Chem. Phys.*, 4, 51–63, 2004.
- Stohl, A.: Computation, accuracy and applications of trajectories - a review and bibliography, *Atmos. Environ.*, 32, 947–966, 1998.
- Stohl, A., Wotawa, G., Seibert, P. and Kromp-Kolb, H.: Interpolation errors in wind fields as a function of spatial and temporal resolution and their impact on different types of kinematic trajectories, *J. Appl. Meteorol.*, 34, 2149–2165, 1995.
- Stohl, A., Hittenberger, M., and Wotawa, G.: Validation of the Lagrangian particle dispersion model FLEXPART against large scale tracer experiment data, *Atmos. Environ.*, 32, 4245–4264, 1998.
- Stohl, A., and Thomson, D. J.: A density correction for Lagrangian particle dispersion models, *Boundary-Layer Meteorol.*, 90, 155–167, 1999.
- Stohl, A., Eckhardt, S., Forster, C., James, P., Spichtinger, N., and Seibert, P.: A replacement for simple back trajectory calculations in the interpretation of atmospheric trace substance measurements, *Atmos. Environ.*, 36, 4635–4648, 2002.
- Stohl, A., Forster, C., Eckhardt, S., Spichtinger, N., Huntrieser, H., Heland, J., Schlager, H., Wilhelm, S., Arnold, F., and Cooper, O.: A backward modeling study of intercontinental pollution transport using aircraft measurements, *J. Geophys. Res.*, 108, 4370, doi:10.1029/2002JD002862, 2003.
- Stohl, A., Forster, C., Frank, A., Seibert, P., and Wotawa, G.: Technical note: The Lagrangian particle dispersion model FLEXPART version 6.2., *Atmos. Chem. Phys.*, 5, 2461–2474, 2005.
- Stohl, A., Forster, C., Huntrieser, H., Mannstein, H., McMillan, W. W., Petzold, A., Schlager, H., and Weinzierl, B.: Aircraft measurements over Europe of an air pollution plume from Southeast Asia – aerosol and chemical characterization, *Atmos. Chem. Phys.*, 7, 913–937, 2007.
- Stohl, A., Berg, T., Burkhardt, J. F., Fjæraa, A. M., Forster, et al.: Arctic smoke – record high air pollution levels in the European Arctic due to agricultural fires in Eastern Europe, *Atmos. Chem. Phys.*, 7, 511–534, 2007.
- Vestreng, V., Breivik, K., Adams, M., Wagner, A., Goodwin, J., Rozovskaya, O., and Pacyna, J. M.:

Emission data reported to LRTAP Convention and NEC Directive – Initial review for HMs and POPs, EMEP Report 2005, Norwegian Meteorological Institute, ISSN 0804-2446, 2005.

Wernli, H., and Davies, H. C.: A Lagrangian-based analysis of extratropical cyclones. I: The method and some applications, *Q. J. R. Meteorol. Soc.*, 123, 467–489, 1997.

White, P. W. (ed.): IFS Documentation, ECMWF, Reading, UK, 2002.

Figure Captions

Fig. 1. Internet homepage produced for a number of concurrent campaigns in spring 2006. Listed are the products available for a number of flights of the NCAR C-130, NASA DC-8 and DLR Falcon aircraft, as well as measurements at the Zeppelin research station on Spitsbergen. For brevity, the number of available data sets has been reduced here as compared to the actual webpage.

Fig. 2. Internet webpage listing the model products available for the Zeppelin research station in May 2006.

Fig. 3. Internet webpage showing the column-integrated PES for the Zeppelin research station on 2 May 2006, 21-24 UTC. The internet page also shows the navigation links available.

Fig. 4. Internet webpage showing the footprint PES for the Zeppelin research station on 2 May 2006, 21-24 UTC.

Fig. 5. Internet webpage showing the anthropogenic carbon monoxide potential source contribution map for the Zeppelin research station on 2 May 2006, 21-24 UTC.

Fig. 6. Internet webpage showing the biomass burning carbon monoxide potential source contribution map for the Zeppelin research station on 2 May 2006, 21-24 UTC.

Fig. 7. Internet webpage showing the retroplume summary plot for the calculation ending at the Zeppelin research station on 2 May 2006, 21-24 UTC.

Fig. 8. Internet webpage showing the age spectra time series of the calculated biomass burning CO mixing ratio at the Zeppelin research station for the month of May 2006.

Figures



Norwegian Institute for Air Research



The NILU Atmospheric Backward Transport Analysis Products for MILAGRO, INTEX-B, IMPACT, MEGAPLUME

by Andreas Stohl

What this site is about

This site presents a resource to interpret transport processes and how they influenced aircraft measurements during recent aircraft campaigns (MILAGRO, INTEX-B, IMPACT, MEGAPLUME). It attempts to replace trajectory calculations -- to date, the major tool used for that purpose -- with quantitative dispersion model runs including full turbulence and convection parameterizations. The plots shown are from backward model runs using the [FLEXPART](#) model. A description of the various products derived from the backward runs can be found [here](#).

Disclaimer: I make these products freely accessible. If you feel that using them contributed significantly to one of your publications, I would appreciate if you could acknowledge that, or offer co-authorship, depending on how important you feel that these products actually were for your work. This will allow us continuing this kind of service also in the future. Of course, on request I can also produce custom-made plots with adjusted plotting domains, better image quality, etc.

Backward modeling products are available for the following flights and other data sets:

C-130

[2006 03 04](#)
[2006 03 08](#)
[2006 03 10](#)
[2006 03 12](#)
[2006 03 16](#)
[2006 03 18](#)
[2006 03 19](#)
[2006 03 22](#)

DC-8

[2006 02 22](#)
[2006 02 24](#)
[2006 03 04](#)
[2006 03 09](#)
[2006 03 11](#)

Falcon

[2006 03 24a](#)
[2006 03 24b](#)
[2006 03 24c](#)
[2006 03 25a](#)
[2006 04 03a](#)

Zeppelin mountain, Spitsbergen

[2006 04](#)
[2006 05](#)

Vertical profiles above Spitsbergen

[Ozone sonde on 2006 05 03, 10:50 UTC](#)
[Profile at 2006 05 03, 0 UTC](#)

If you have any questions about the modelling products please contact [Andreas Stohl](#).

Fig. 1. Internet homepage produced for a number of concurrent campaigns in spring 2006. Listed are the products available for a number of flights of the NCAR C-130, NASA DC-8 and DLR Falcon aircraft, as well as measurements at the Zeppelin research station on Spitsbergen. For brevity, the number of available data sets has been reduced here as compared to the actual webpage.

Zeppelin_200605

[RETURN TO FLEXPART BACKWARD RUNS HOME PAGE](#)

ECMWF DATA	GFS DATA
EMISSION TRACER TIME SERIES, TOTAL	EMISSION TRACER TIME SERIES, TOTAL
EMISSION TRACER TIME SERIES, AGESPECTRUM TOTAL	EMISSION TRACER TIME SERIES, AGESPECTRUM TOTAL
EMISSION TRACER TIME SERIES, NORTH AMERICAN	EMISSION TRACER TIME SERIES, NORTH AMERICAN
EMISSION TRACER TIME SERIES, ASIAN	EMISSION TRACER TIME SERIES, ASIAN
EMISSION TRACER TIME SERIES, EUROPEAN	EMISSION TRACER TIME SERIES, EUROPEAN
EMISSION TRACER TIME SERIES, AFRICAN	EMISSION TRACER TIME SERIES, AFRICAN
EMISSION TRACER TIME SERIES, SOUTH AMERICAN	EMISSION TRACER TIME SERIES, SOUTH AMERICAN
EMISSION TRACER TIME SERIES, AUSTRALIAN	EMISSION TRACER TIME SERIES, AUSTRALIAN
FIRE EMISSION TRACER TIME SERIES	FIRE EMISSION TRACER TIME SERIES
RETROPLUME SUMMARY, GLOBAL	RETROPLUME SUMMARY, GLOBAL
RETROPLUME SUMMARY, REGIONAL	RETROPLUME SUMMARY, REGIONAL
RETROPLUME SUMMARY, LOCAL	RETROPLUME SUMMARY, LOCAL
COLUMN RESIDENCE TIME, GLOBAL	COLUMN RESIDENCE TIME, GLOBAL
COLUMN RESIDENCE TIME, REGIONAL	COLUMN RESIDENCE TIME, REGIONAL
COLUMN RESIDENCE TIME, LOCAL	COLUMN RESIDENCE TIME, LOCAL
FOOTPRINT RESIDENCE TIME, GLOBAL	FOOTPRINT RESIDENCE TIME, GLOBAL
FOOTPRINT RESIDENCE TIME, REGIONAL	FOOTPRINT RESIDENCE TIME, REGIONAL
FOOTPRINT RESIDENCE TIME, LOCAL	FOOTPRINT RESIDENCE TIME, LOCAL
CO SOURCE CONTRIBUTION, GLOBAL	CO SOURCE CONTRIBUTION, GLOBAL
CO SOURCE CONTRIBUTION, REGIONAL	CO SOURCE CONTRIBUTION, REGIONAL
CO SOURCE CONTRIBUTION, LOCAL	CO SOURCE CONTRIBUTION, LOCAL
NO2 SOURCE CONTRIBUTION, GLOBAL	NO2 SOURCE CONTRIBUTION, GLOBAL
NO2 SOURCE CONTRIBUTION, REGIONAL	NO2 SOURCE CONTRIBUTION, REGIONAL
NO2 SOURCE CONTRIBUTION, LOCAL	NO2 SOURCE CONTRIBUTION, LOCAL
SO2 SOURCE CONTRIBUTION, GLOBAL	SO2 SOURCE CONTRIBUTION, GLOBAL
SO2 SOURCE CONTRIBUTION, REGIONAL	SO2 SOURCE CONTRIBUTION, REGIONAL
SO2 SOURCE CONTRIBUTION, LOCAL	SO2 SOURCE CONTRIBUTION, LOCAL
FIRE CO SOURCE CONTRIBUTION, GLOBAL	FIRE CO SOURCE CONTRIBUTION, GLOBAL
FIRE CO SOURCE CONTRIBUTION, REGIONAL	FIRE CO SOURCE CONTRIBUTION, REGIONAL
FIRE CO SOURCE CONTRIBUTION, LOCAL	FIRE CO SOURCE CONTRIBUTION, LOCAL

Fig. 2. Internet webpage listing the model products available for the Zeppelin research station in May 2006.

HOME	AVAILABLE PRODUCTS FOR THIS FLIGHT				PLOT USING GFS DATA		
CHANGE TYPE OF PLOT:	retroplume	column	footprint	co	no2	so2	fire_co
CHANGE DOMAIN OF PLOT:	global		regional		local		
NAVIGATE IN TIME:	PREVIOUS		NEXT		OVERVIEW		

column-integrated emission sensitivity in nested domain for Zeppelin_200605

Start time of sampling 20060502.210000 End time of sampling 20060503. 0

Lower release height 478 m Upper release height 478 m

Meteorological data used are from ECMWF

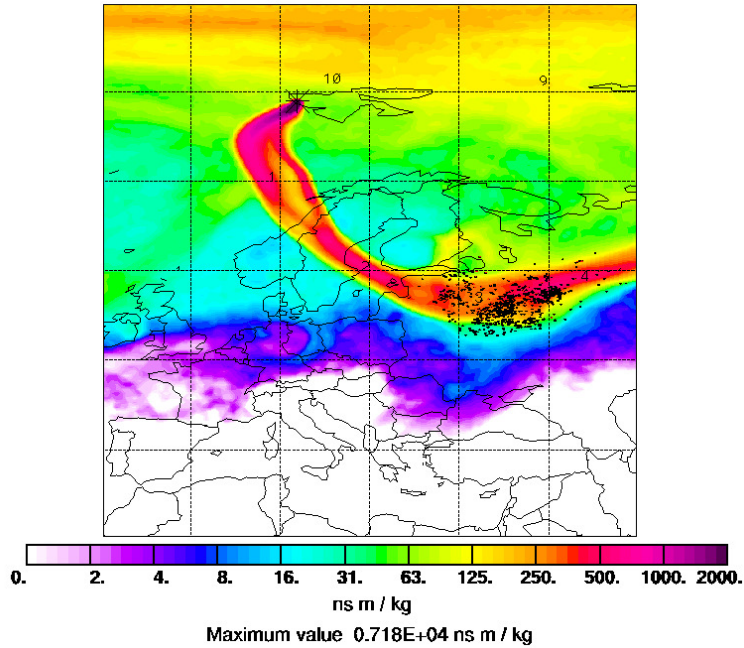


Fig. 3. Internet webpage showing the column-integrated PES for the Zeppelin research station on 2 May 2006, 21-24 UTC. The internet page also shows the navigation links available.

HOME	AVAILABLE PRODUCTS FOR THIS FLIGHT				PLOT USING GFS DATA			
CHANGE TYPE OF PLOT:	retroplume	column	footprint	co	no2	so2	fire_co	
CHANGE DOMAIN OF PLOT:	global			regional		local		
NAVIGATE IN TIME:	PREVIOUS			NEXT		OVERVIEW		

Footprint emission sensitivity in nested domain for c130 060322

Start time of sampling 20060502.210000 End time of sampling 20060503. 0

Lower release height 478 m Upper release height 478 m

Meteorological data used are from ECMWF

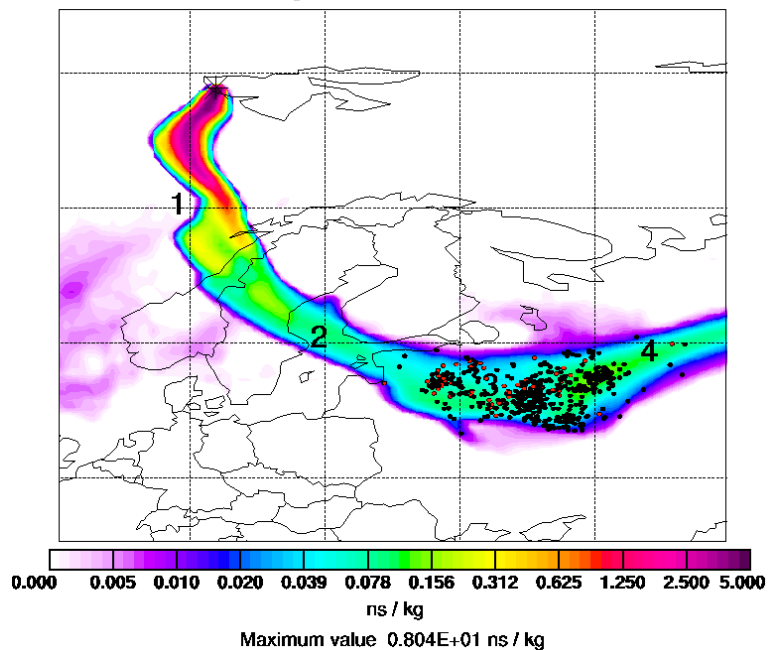


Fig. 4. Internet webpage showing the footprint PES for the Zeppelin research station on 2 May 2006, 21-24 UTC.

HOME	AVAILABLE PRODUCTS FOR THIS FLIGHT				PLOT USING GFS DATA		
CHANGE TYPE OF PLOT:	retroplume	column	footprint	co	no2	so2	fire_co
CHANGE DOMAIN OF PLOT:	global			regional		local	
NAVIGATE IN TIME:	PREVIOUS		NEXT		OVERVIEW		

CO source contributions in nested domain for Zeppelin_200605

Start time of sampling 20060502.210000 End time of sampling 20060503. 0

Lower release height 478 m Upper release height 478 m

Meteorological data used are from ECMWF

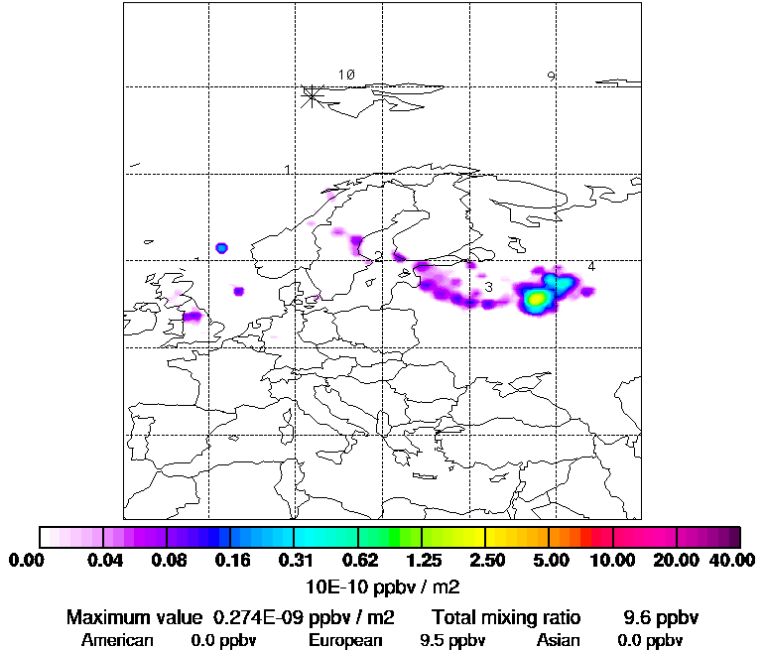


Fig. 5. Internet webpage showing the anthropogenic carbon monoxide potential source contribution map for the Zeppelin research station on 2 May 2006, 21-24 UTC.

HOME	AVAILABLE PRODUCTS FOR THIS FLIGHT				PLOT USING GFS DATA			
CHANGE TYPE OF PLOT:	retroplume	column	footprint	co	no2	so2	fire_co	
CHANGE DOMAIN OF PLOT:	global			regional		local		
NAVIGATE IN TIME:	PREVIOUS			NEXT		OVERVIEW		

Fire CO source contributions in nested domain for Zeppelin_200605

Start time of sampling 20060502.210000 End time of sampling 20060503. 0

Lower release height 478 m Upper release height 478 m

Meteorological data used are from ECMWF

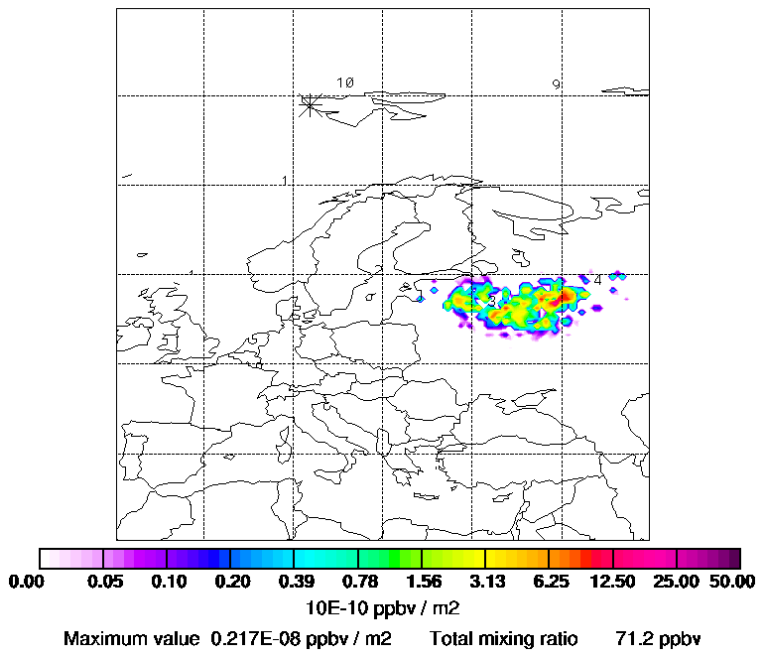


Fig. 6. Internet webpage showing the biomass burning carbon monoxide potential source contribution map for the Zeppelin research station on 2 May 2006, 21-24 UTC.

HOME	AVAILABLE PRODUCTS FOR THIS FLIGHT				PLOT USING GFS DATA		
CHANGE TYPE OF PLOT:	retroplume	column	footprint	co	no2	so2	fire_co
CHANGE DOMAIN OF PLOT:	global			regional		local	
NAVIGATE IN TIME:	PREVIOUS			NEXT		OVERVIEW	

Retroplume summary for Zeppelin_200605

Start time of sampling 20060502.210000 End time of sampling 20060503. 0
Meteorological data used is ECMWF

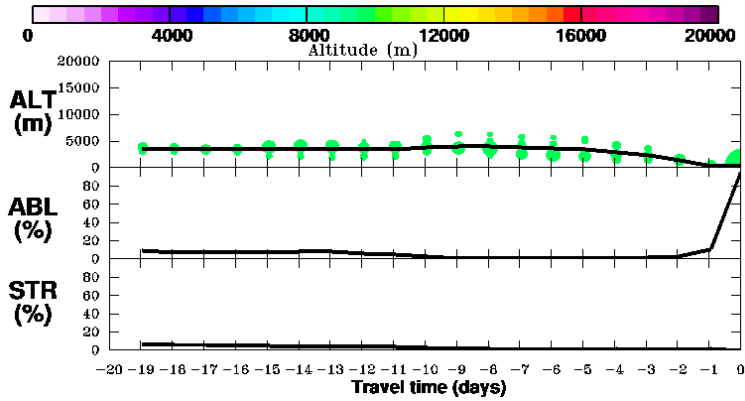
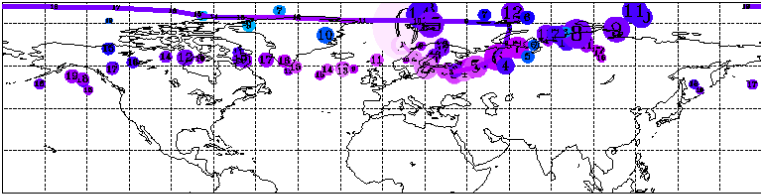


Fig. 7. Internet webpage showing the retroplume summary plot for the calculation ending at the Zeppelin research station on 2 May 2006, 21-24 UTC.

RETURN TO FLEXPART BACKWARD RUNS HOMEPAGE	AVAILABLE PRODUCTS FOR THIS DATA SET
CO tracer data	

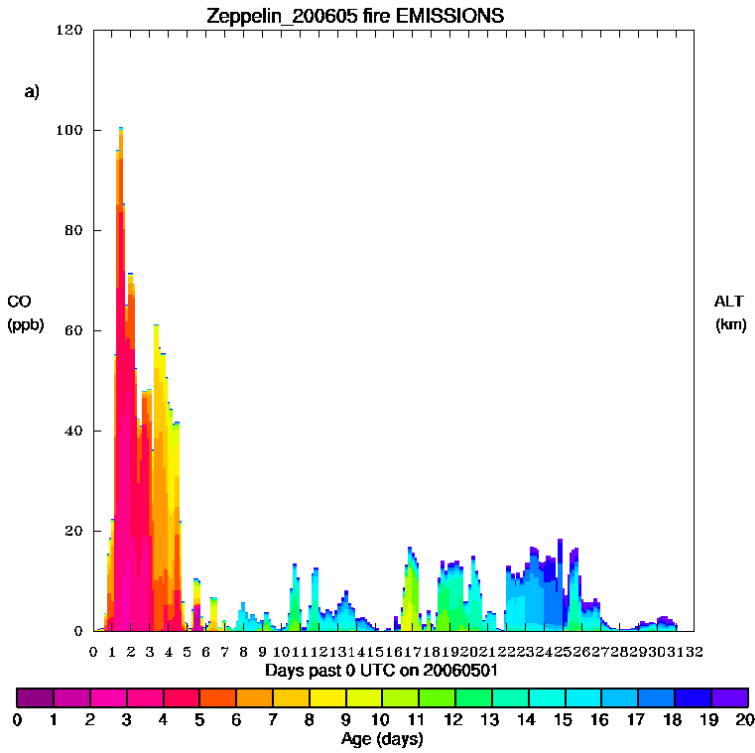


Fig. 8. Internet webpage showing the age spectra time series of the calculated biomass burning CO mixing ratio at the Zeppelin research station for the month of May 2006.